Analysis of Transient Scattering From Composite Arbitrarily Shaped Complex Structures

Tapan Kumar Sarkar, *Fellow, IEEE*, Wonwoo Lee, and Sadasiva M. Rao, *Fellow, IEEE*

***Abstract*—A time-domain surface integral equation approach based on the electric field formulation is utilized to calculate the transient scattering from both conducting and dielectric bodies consisting of arbitrarily shaped complex structures. The solution method is based on the method of moments (MoM) and involves the modeling of an arbitrarily shaped structure in conjunction with the triangular patch basis functions. An implicit method is described to solve the coupled integral equations derived utilizing the equivalence principle directly in the time domain. The usual late-time instabilities associated with the time-domain integral equations are avoided by using an implicit scheme. Detailed mathematical steps are included along with representative numerical results.**

***Index Terms*—Electromagnetic (EM) scattering, integral equations, transient EM analysis.**

I. Introduction

When broad-band information is desired it is more efficient to solve for the electromagnetic (EM) scattering problem in the time domain. Some of the early analytical works in transient EM problems were based on physical optics to obtain the approximate impulse response from conducting flat plates, spheres, and prolate spheroids [1], [2]. A time-domain solution for an infinite cylindrical antenna was performed by Wu [3]. Rigorous expressions have also been obtained for a dipole in the presence of a conducting wedge [4], an infinite circular cylinder [5], a semi-infinite cone [6], and a circular disk [7] to name a few.

Mitzner [31] and Shaw [32] applied the marching-on-in-time method for solving integral equations. Bennett extended the formulation using an integro-differential equation obtained by enforcing the boundary conditions of the tangential field components on the surface of the scatterer could be solved for directly in the time domain [8]. Thus, Bennett generalized the technique from acoustics and EMs. This technique has been labeled the marching-on-in-time (MOT) algorithm or the time-domain integral-equation (TDIE) technique. Like method of moments (MoM), the MOT method discretizes the scatterer into segments or patches. The time axis is generally divided into equal increments. With this method, the currents on the scatterer at a certain time $t = t_1$ are related to the currents on the scatterer at $t < t_1$. This is because the "effect" of a current requires a finite time to "travel" to the observation point. By properly choosing a time step, an explicit solution for the present-time currents may be obtained which may be solved recursively. So, once the currents at t_1 are determined, the time is incremented to the next interval and the procedure is repeated. Since the present-time currents are functions of previously occurring currents, the currents need to be stored in a current history matrix.

In this work, the transient scattering from arbitrarily shaped, composite three-dimensional (3-D), developed bodies is considered using the time-domain integral equation (TDIE). TDIE has been solved earlier using the MOT techniques for conducting structures [8]–[15]. However, only Tijhuis [16], Vechinski and Rao [17], [18], and Mieras and Bennett [19] used the technique to calculate scattering from dielectric structures. In [16] and [25], a domain formulation for inhomogeneous objects was considered as opposed to the surface formulation described here. In particular, Mieras and Bennett solved the 3-D dielectric body problem. However, their mathematical formulation resulted in the simultaneous solution of four integral equations. Furthermore, their usage of rectangular patches restricted the modeling capabilities.

Even though the use of triangular patches to model arbitrary surfaces [20]–[22] provides flexibility, the problem with the TDIE is that it becomes unstable for late times. During the last few years many methods [23]–[28] have appeared in the literature that deal with the numerical instability problem. What is needed is a satisfactory scheme which will work under all circumstances is still elusive.

That is why an implicit scheme [29], [33], [34] has been applied to take care of late-time instabilities. Transient scattering from an aircraft is presented to illustrate the efficacy of this procedure. The aircraft has a nose which is made of dielectric and the remainder is conducting as shown in Fig. 1.

In Section II, the time-domain electric field integral equation is presented. Section III describes the triangular patch basis functions and in Section IV the numerical implementation is developed. Section V contains the expressions for the far scattered field. Section VI presents numerical examples followed by Section VII, the conclusion.

II. Surace Integral Equation

In this section, we describe the development of integral equations in terms of unknown equivalent currents on the conductors/dielectric bodies illuminated by a transient EM pulse using the equivalence principle.

Consider a system of finite length, finite or zero-thickness conductors situated in the presence of several dielectric bodies

Manuscript received September 1, 1999; revised April 21, 2000. This work was supported in part by SPAWAR Systems under Contract N66001-99-1-8922.

T. K. Sarkar and W. Lee are with the Department of Electrical Engineering and Computer Science, Syracuse University, Syracuse, NY 13244 USA (e-mail: tksarkar@syr.edu).

S. M. Rao is with the Department of Electrical Engineering, Auburn University, Auburn, AL 36849 USA.

Publisher Item Identifier S 0018-926X(00)09377-7.

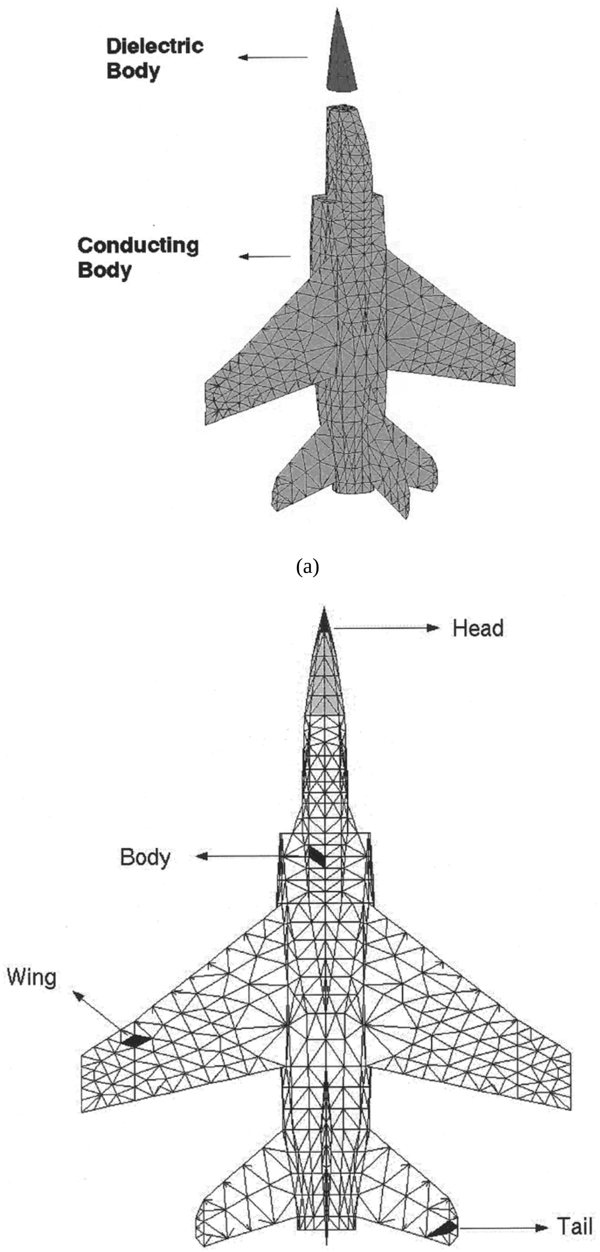

Fig. 1. (a) An aircraft. (b) Locations on the aircraft where the transient currents are computed.

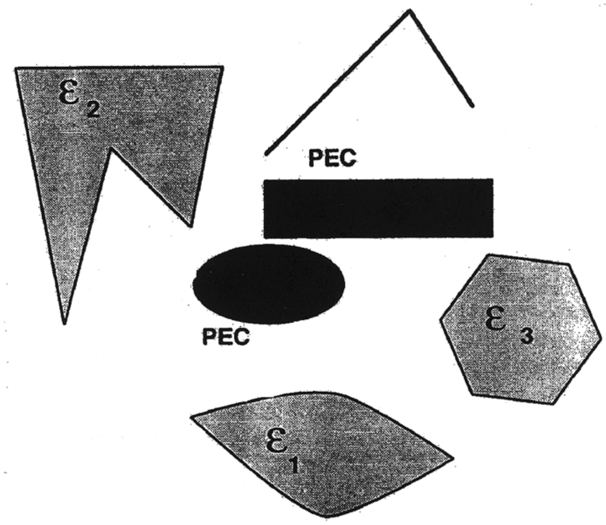

Fig. 2. Conducting and dielectric bodies in a homogeneous medium.

as shown in Fig. 2. The whole system is immersed in free-space and is illuminated by a transient pulse. In the present formulation, the central idea is that we treat each conductor and each dielectric body as if it is immersed in free-space. Thus, we consider a combination of conductor-dielectric interface as two bodies separated by zero distance. In this way, we treat all dielectric bodies as closed structures whereas the conducting bodies may be open or closed. Since there may be zero-thickness conductors we employ only the electric field formulation to treat both conductors and dielectrics.

For the sake of presentation, we assume that there is one conducting body and one dielectric body. However, the formulation is quite general and can be used to analyze multiple complex structures.

By using the equivalence principle, we replace the conducting structures by an equivalent surface current $\mathbf{J}_c$ radiating in free-space. On all the conductor surfaces S_c the tangential component of the electric field must approach zero. The total tangential electric field on the conducting surface must be zero. The regions exterior and interior to the dielectric body are characterized by medium parameters (μ_e, ε_e) and (μ_d, ε_d), respectively. It may be noted that the incident field is defined to be that which would exist in space if the structure was not present. Further, we assume that the dielectric body is a closed body so that a unique outward normal vector can be defined unambiguously. We employ the equivalence principle [19], [30] to split the original problem into two separate ones. The first one is where the fields are equivalent external to the body and the second one is where the fields are equivalent internal to the body. The original problem is shown in Fig. 3 and the equivalent exterior problem in Fig. 4. In the first case, we establish the restriction that only the fields exterior to the body remain the same. Therefore we are free to choose what the interior fields are to be. For simplicity, the interior fields are set to zero, and then the interior material parameters are set to be the same as those external to the body. Now, since the tangential components of the fields are not continuous across the dielectric surface S_d (in the equivalent problem), equivalent electric currents $\mathbf{J}_d$ and magnetic currents $\mathbf{M}_d$ are required to make up for the discontinuity. Since these currents now radiate in a homogeneous unbounded medium, one can use the free space Green's function to compute the fields, utilizing the vector and scalar potentials. So, if we take any point C just inside the surface S_d, then we require that the sum of the incident field and the scattered field (due to the currents $\mathbf{J}_d$ & $\mathbf{M}_d$) add to zero. Let S_d^- designate points just inside the surface S_d, then the total electric fields satisfy

$$\mathbf{E}_{\tan} = 0 \text{ on } S_d^- \tag{1}$$

where the superscript "$-$" refers to a surface internal to S_d and "$+$" denotes a surface external to S_d.

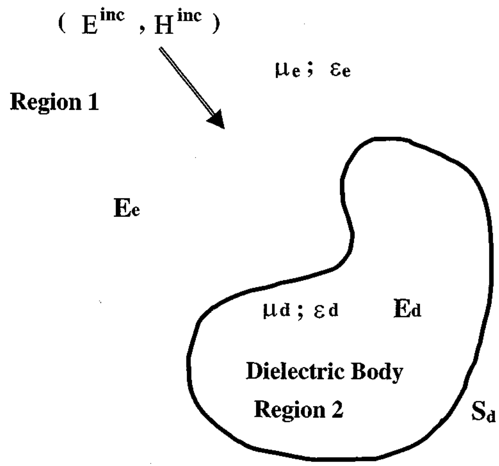

Fig. 3. Original problem.

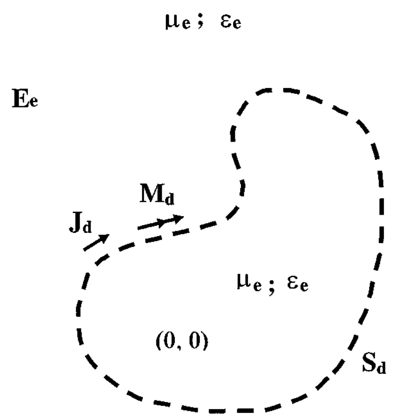

Fig. 4. External equivalence problem.

Similarly, we can form an equivalent interior problem as shown in Fig. 5. In this case, the external fields are set equal to zero and, hence, the exterior material parameters are the same as the interior parameters of the dielectric body. As before equivalent currents along the surface internal to S_d are set up to satisfy the discontinuity in the fields. It turns out that these equivalent currents are just the negative of the currents for the exterior equivalent problem. Here, we require that these currents radiate zero fields external to the body.

Therefore, a set of coupled integral equations may be written for the tangential component of the total electric field in terms of the equivalent currents $\mathbf{J}_c$ on the conducting structure and $\mathbf{J}_d$ and $\mathbf{M}_d$ on the dielectric structure given by

$$\left[\mathbf{E}_e^s(\mathbf{J}_c,\, \mathbf{J}_d,\, \mathbf{M}_d) + \mathbf{E}^{\text{inc}}\right]_{\tan} = 0 \quad \mathbf{r} \in S_c \tag{2}$$

$$\left[\mathbf{E}_e^s(\mathbf{J}_c,\, \mathbf{J}_d,\, \mathbf{M}_d) + \mathbf{E}^{\text{inc}}\right]_{\tan} = 0 \; \mathbf{r} \in S_d^- \tag{3}$$

$$\left[\mathbf{E}_d^s(-\mathbf{J}_d,\, -\mathbf{M}_d)\right]_{\tan} = 0 \quad \mathbf{r} \in S_d^+ \tag{4}$$

where $\mathbf{E}^{\text{inc}}$ represents the incident field and the subscripts "e" and "d" represent the fields of the exterior and interior equivalence models evaluated at the boundaries of the equivalence regions in the limits as they are approached from their complementary regions, respectively. Hence

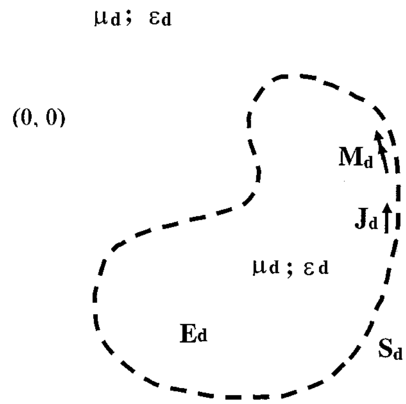

Fig. 5. Internal equivalence problem.

$$\mathbf{E}_v^s[\mathbf{J}] = \mp \frac{\partial \mathbf{A}_v}{\partial t} \mp \nabla \Phi_v \tag{5}$$

$$\mathbf{E}_v^s[\mathbf{M}] = \mp \frac{1}{\varepsilon_v} \nabla \times \mathbf{F}_v \tag{6}$$

where $\mathbf{A}_v$ and $\mathbf{F}_v$ are the magnetic and electric vector potentials, respectively, and Φ_v is the electric scalar potential given by

$$\mathbf{A}_v(\mathbf{r},\, t) = \mu_v \int_S \frac{\mathbf{J}\left(\mathbf{r}',\, t - \dfrac{R}{c_v}\right)}{4\pi R}\, dS' \tag{7}$$

$$\mathbf{F}_v(\mathbf{r},\, t) = \varepsilon_v \int_S \frac{\mathbf{M}\left(\mathbf{r}',\, t - \dfrac{R}{c_v}\right)}{4\pi R}\, dS' \tag{8}$$

$$\Phi_v(\mathbf{r},\, t) = \frac{1}{\varepsilon_v} \int_S \frac{q_s\left(\mathbf{r}',\, t - \dfrac{R}{c_v}\right)}{4\pi R}\, dS'. \tag{9}$$

For $v =$ the exterior region (denoted by e), the signs in (5) and (6) is "$-$," whereas when $v =$ the interior region (denoted by d), then the sign in (5) and (6) is "+." S is the surface of integration. c_v is the velocity of wave propagation in medium v. $R = |\mathbf{r} - \mathbf{r}'|$ is the distance from the field point $\mathbf{r}$ to the source point $\mathbf{r}'$. The electric surface charge density q_s is related to the electric surface current density by the continuity equation given by

$$\nabla \cdot \mathbf{J} = -\frac{\partial q_s}{\partial t} \Rightarrow q_s = -\int_{\tau=0}^{t} \nabla \cdot \mathbf{J}\, d\tau. \tag{10}$$

Note that in (7), $\mathbf{J}$ refers to either $\mathbf{J}_c$ or $\mathbf{J}_d$ when $v =$ exterior region. However, when $v =$ interior region, $\mathbf{J} = \mathbf{J}_d$ because for this case $\mathbf{J}_d$ affects only the internal fields. Also, note that the time retardation R/c_v depends upon the medium in which the field is evaluated. By using (10), (9) may be rewritten as

$$\Phi_v(\mathbf{r},\, t) = -\frac{1}{\varepsilon_v} \int_S \int_{\tau=0}^{t} \frac{\nabla \cdot \mathbf{J}\left(\mathbf{r}',\, \tau - \dfrac{R}{c_v}\right)}{4\pi R}\, d\tau\, dS'. \tag{11}$$

By enforcing the continuity conditions, we note that on the surface S_c, $\mathbf{E}^s_{e,\tan} = -\mathbf{E}^{\rm inc}_{\tan}$ and on the surface S_d we have

$$\mathbf{E}^{S_d^-}_{e,\tan} = -\mathbf{E}^{\rm inc}_{\tan}; \quad \mathbf{E}^{S_d^+}_{d,\tan} = 0$$

where the subscript "$\tan$" refers to the tangential components of the fields. Thus, we derive the following set of integral equations for the composite body problem given by

$$\left[\frac{\partial \mathbf{A}_e}{\partial t} + \nabla\Phi_e + \frac{1}{\varepsilon_e}\nabla\times\mathbf{F}_e\right]_{\tan} = \left[\mathbf{E}^{\rm inc}\right]_{\tan,} \quad \text{for } \mathbf{r}\in S_c \tag{12}$$

$$\left[\frac{\partial \mathbf{A}_e}{\partial t} + \nabla\Phi_e + \frac{1}{\varepsilon_e}\nabla\times\mathbf{F}_e\right]_{\tan} = \left[\mathbf{E}^{\rm inc}\right]_{\tan,} \quad \text{for } \mathbf{r}\in S_d^- \tag{13}$$

$$\left[\frac{\partial \mathbf{A}_d}{\partial t} + \nabla\Phi_d + \frac{1}{\varepsilon_d}\nabla\times\mathbf{F}_d\right]_{\tan} = 0 \quad \text{for } \mathbf{r}\in S_d^+. \tag{14}$$

The integral equation described by (12)–(14) is the electric field integral equations (EFIE) since we enforced the continuity condition on electric field only.

III. Description of the Basis Function

In this work, the given complex structures are approximated by planar triangular patches. The triangular patches have the ability to conform to any geometrical surface or boundary, permit easy descriptions of the patching scheme to the computer and may be used with greater densities on those portions of the surface where more resolution is desired. Assuming a suitable triangulation for the scattering structure, two sets of basis functions are defined to approximate $\mathbf{J}$ and $\mathbf{M}$ as follows.

Fig. 6 shows two triangles T_n^p and T_n^q, associated with the nth edge of a triangulated surface modeling the surface of a body. Points in T_n^p may be designated either by the position vector $\mathbf{r}$, or by $\boldsymbol{\rho}_n^p$ defined with respect to the free vertex of T_n^p. Similar remarks apply to the position vector $\mathbf{r}$ in T_n^q except that it is directed toward the free vertex. It is assumed that the index $p < q$ and, thus, the reference direction for the positive current associated with the nth edge is from T_n^p to T_n^q.

Referring to Fig. 7, we define the two vector basis functions associated with the nth edge as

$$\mathbf{f}_n(\boldsymbol{\rho}) = \begin{cases} \dfrac{\boldsymbol{\rho}_n^p}{h_n^p} & \boldsymbol{\rho}_n^p \in T_n^p \\ \dfrac{\boldsymbol{\rho}_n^q}{h_n^q} & \boldsymbol{\rho}_n^q \in T_n^q \\ 0, & \text{otherwise} \end{cases} \tag{15}$$

and

$$\mathbf{g}_n(\boldsymbol{\rho}) = \begin{cases} \dfrac{\mathbf{a}_n^p \times \boldsymbol{\rho}_n^p}{h_n^p} & \boldsymbol{\rho}_n^p \in T_n^p \\ \dfrac{\mathbf{a}_n^q \times \boldsymbol{\rho}_n^q}{h_n^q} & \boldsymbol{\rho}_n^q \in T_n^q \\ 0, & \text{otherwise} \end{cases} \tag{16}$$

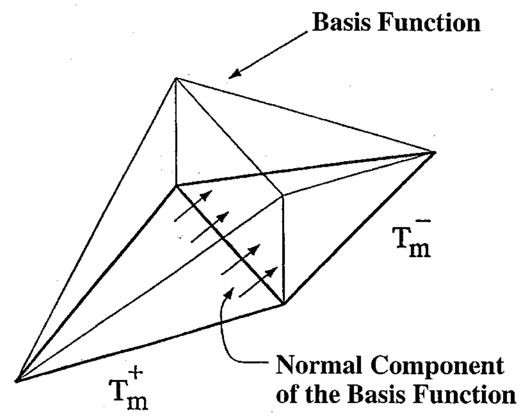

Fig. 6. Geometrical description of the basis function.

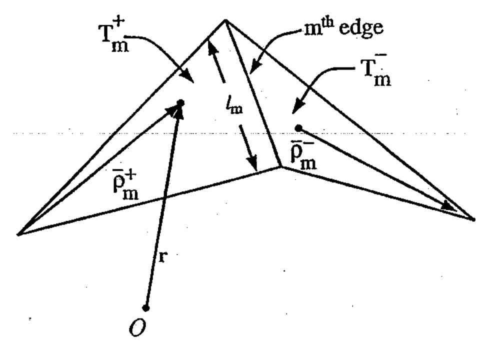

Fig. 7. Triangles associated with an edge.

where h_n^p and $\mathbf{a}_n^p$ are the height of the edge from the free vertex and the unit normal vector to the plane of triangle T_n^p, respectively. Similar remarks apply to the quantities in triangle T_n^q.

The electric current $\mathbf{J}$ and the magnetic current $\mathbf{M}$ on the scattering structure may be approximated in terms of the two basis functions as

$$\mathbf{J} = \sum_{n=1}^{N_c+N_d} \mathbf{I}_n\mathbf{f}_n \quad \mathbf{M} = \sum_{n=1}^{N_d} \mathbf{M}_n\mathbf{g}_n \tag{17}$$

where N_c and N_d represent the number of edges, discounting the boundary edges in the triangulated model of the conducting and the dielectric object, respectively. Thus, for a composite body problem, we have $N = N_c + 2N_d$ unknowns in the MoM solution procedure. It may be noted that the functions $\mathbf{f}_n$ are the functions described in [20]. The functions $\mathbf{g}_n$ are point-wise orthogonal to $\mathbf{f}_n$ in the triangle pair and usage of this orthogonality property provides a better stability in the numerical solution.

IV. Numerical Solution Procedure

First of all, for the numerical solution we divide the time axis into equal intervals of Δt and refer $t_j = j\Delta t$. Next, we assume that all the current coefficients are zero for $t \le 0$ which implies that we are seeking a causal solution. We also assume that, when calculating unknown coefficients $I_n(t)$ and $M_n(t)$ at $t = t_j$, the coefficients for all the previous time instants are known.

Next, by approximating the time derivative in (12)–(14) and using the standard backward difference formula, we have at $t = t_j$

$$\left[\mathbf{A}_e(\mathbf{r}, t_j) + (\Delta t)\nabla\Phi_e(\mathbf{r}, t_j) + \frac{\Delta t}{\varepsilon_e}\nabla\times\mathbf{F}_e(\mathbf{r}, t_j)\right]_{\tan} = \left[(\Delta t)\mathbf{E}^{\rm inc}(\mathbf{r}, t_j) + \mathbf{A}_e(\mathbf{r}, t_{j-1})\right]_{\tan,} \quad \text{for } \mathbf{r}\in S_c \tag{18}$$

$$\left[\mathbf{A}_e(\mathbf{r}, t_j) + (\Delta t)\nabla\Phi_e(\mathbf{r}, t_j) + \frac{\Delta t}{\varepsilon_e}\nabla\times\mathbf{F}_e(\mathbf{r}, t_j)\right]_{\tan} = \left[(\Delta t)\mathbf{E}^{\rm inc}(\mathbf{r}, t_j) + \mathbf{A}_e(\mathbf{r}, t_{j-1})\right]_{\tan,} \quad \text{for } \mathbf{r}\in S_d^- \tag{19}$$

$$\left[\mathbf{A}_d(\mathbf{r}, t_j) + (\Delta t)\nabla\Phi_d(\mathbf{r}, t_j) + \frac{\Delta t}{\varepsilon_d}\nabla\times\mathbf{F}_d(\mathbf{r}, t_j)\right]_{\tan} = \left[\mathbf{A}_d(\mathbf{r}, t_{j-1})\right]_{\tan} \quad \text{for } \mathbf{r}\in S_d^+. \tag{20}$$

Notice that in (18)–(20), the right-hand side consists of known quantities, i.e., the incident field and the vector potential at $t = t_{j-1}$.

We now solve (18)–(20) by applying the Galerkin's method in the MoM context and hence the testing functions are same as the expansion functions. By choosing the expansion functions $\mathbf{f}_m$ also as the testing functions and defining the inner product for two real vector functions $\mathbf{f}$ and $\mathbf{h}$ by

$$\langle\mathbf{f}, \mathbf{h}\rangle = \int_S \mathbf{f}\cdot\mathbf{h}\, dS \tag{21}$$

we have

$$\langle\mathbf{f}_m, \mathbf{A}_e(\mathbf{r}, t_j)\rangle + \langle\mathbf{f}_m, (\Delta t)\nabla\Phi_e(\mathbf{r}, t_j)\rangle + \left\langle\mathbf{f}_m, \frac{(\Delta t)}{\varepsilon_e}\nabla\times\mathbf{F}_e(\mathbf{r}, t_j)\right\rangle = \langle\mathbf{f}_m, (\Delta t)\mathbf{E}^{\rm inc}(\mathbf{r}, t_j)\rangle + \langle\mathbf{f}_m, \mathbf{A}_e(\mathbf{r}, t_{j-1})\rangle \quad \text{for } \mathbf{r}\in S_c \tag{22}$$

$$\langle\mathbf{f}_m, \mathbf{A}_e(\mathbf{r}, t_j)\rangle + \langle\mathbf{f}_m, (\Delta t)\nabla\Phi_e(\mathbf{r}, t_j)\rangle + \left\langle\mathbf{f}_m, \frac{(\Delta t)}{\varepsilon_e}\nabla\times\mathbf{F}_e(\mathbf{r}, t_j)\right\rangle = \langle\mathbf{f}_m, (\Delta t)\mathbf{E}^{\rm inc}(\mathbf{r}, t_j)\rangle + \langle\mathbf{f}_m, \mathbf{A}_e(\mathbf{r}, t_{j-1})\rangle \quad \text{for } \mathbf{r}\in S_d^- \tag{23}$$

$$\langle\mathbf{f}_m, \mathbf{A}_d(\mathbf{r}, t_j)\rangle + \langle\mathbf{f}_m, (\Delta t)\nabla\Phi_d(\mathbf{r}, t_j)\rangle + \left\langle\mathbf{f}_m, \frac{(\Delta t)}{\varepsilon_d}\nabla\times\mathbf{F}_d(\mathbf{r}, t_j)\right\rangle = \langle\mathbf{f}_m, \mathbf{A}_d(\mathbf{r}, t_{j-1})\rangle \quad \text{for } \mathbf{r}\in S_d^+. \tag{24}$$

Consider the testing of the vector potential $\mathbf{A}_v$ and the gradient of scalar potential $\nabla\Phi_v$ in (22)–(24). Here, we have

$$\langle\mathbf{f}_m, \mathbf{A}_v(\mathbf{r}, t_j)\rangle = \int_S \mathbf{f}_m\cdot\mathbf{A}_v(\mathbf{r}, t_j)\, dS \tag{25}$$

$$\langle\mathbf{f}_m, (\Delta t)\Phi_v(\mathbf{r}, t_j)\rangle = (\Delta t)\int_S \mathbf{f}_m\cdot\nabla\Phi_v(\mathbf{r}, t_j)\, dS = -(\Delta t)\int_S \Phi_v(\mathbf{r}, t_j)\nabla\cdot\mathbf{f}_m\, dS. \tag{26}$$

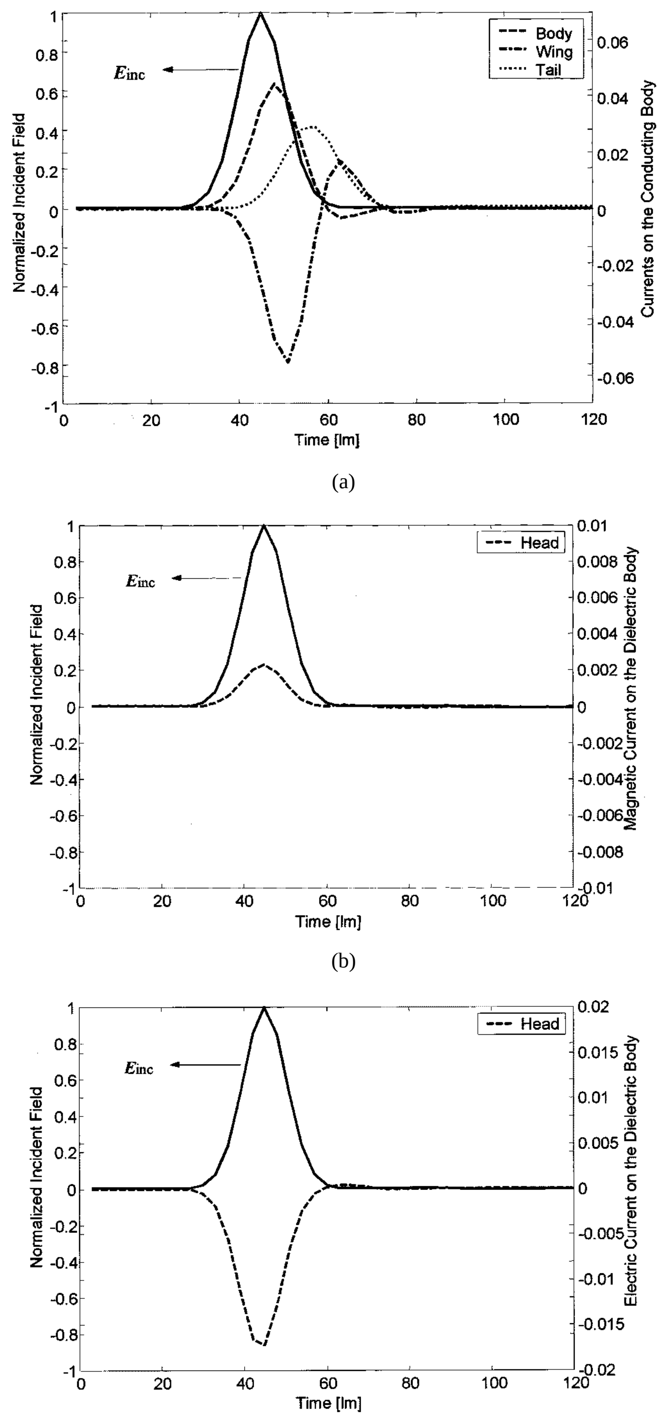

Fig. 8. (a) Electric currents on the conducting structure. (b) Magnetic current on the dielectric part. (c) Electric current on the dielectric part.

Next, we consider the evaluation of $\langle\mathbf{f}_m, (\Delta t/\varepsilon_v)\nabla\times\mathbf{F}_v\rangle$. Using (5) and extracting Cauchy principal value from the curl term, we may rewrite $\langle\mathbf{f}_m, (\Delta t/\varepsilon_v)\nabla\times\mathbf{F}_v\rangle$ as

$$\left\langle\mathbf{f}_m, \left(\frac{\Delta t}{\varepsilon_v}\right)\nabla\times\mathbf{F}_v\right\rangle = \left\langle\mathbf{f}_m, \mp\Delta t\mathbf{a}_n\times\frac{\mathbf{M}}{2}\right\rangle + \left\langle\mathbf{f}_m, \left(\frac{\Delta t}{\varepsilon_v}\right)\nabla\times\underline{\mathbf{F}}_v\right\rangle \tag{27}$$

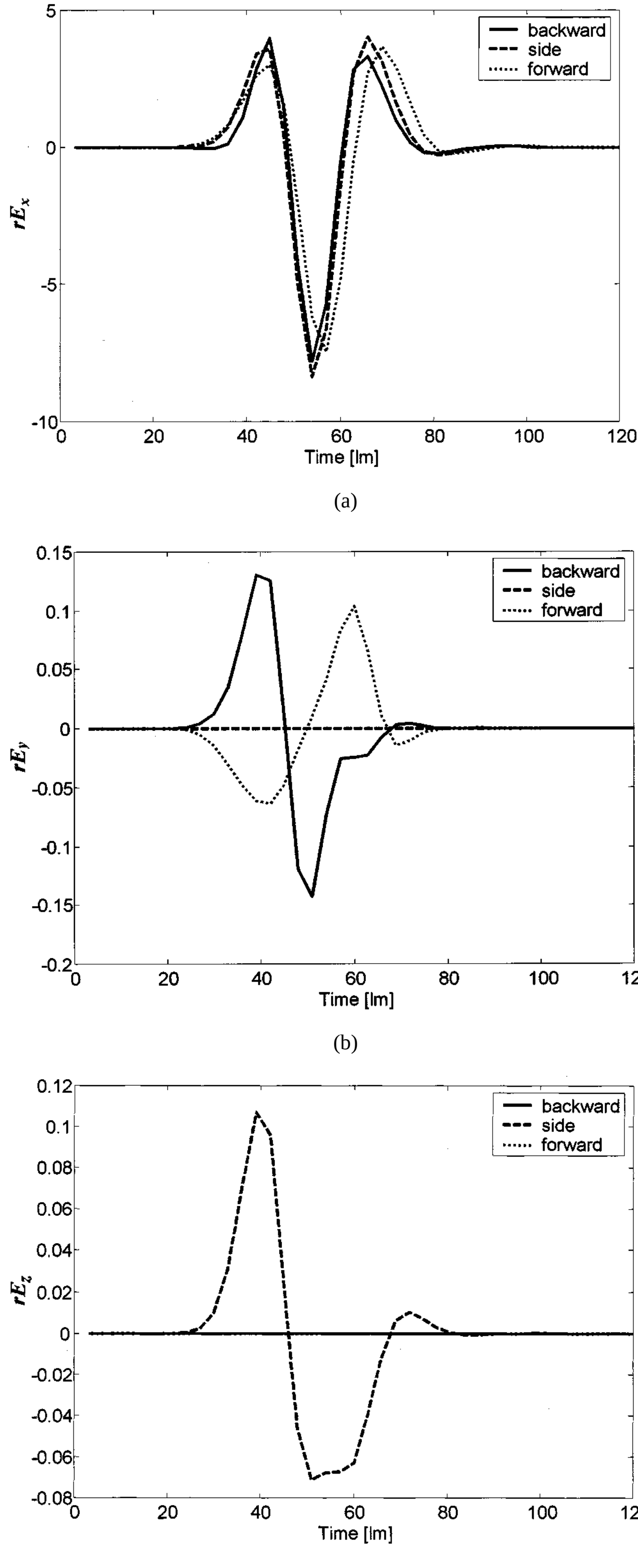

Fig. 9. (a) x component of the scattered far-field along $\phi = 0;\ \theta = 0°$ (backward), $\phi = 0;\ \theta = 180°$ (forward) and $\phi = 90°;\ \theta = 90°$ (side). (b) y component of the scattered far-field along the three previously defined directions. (c) z component of the scattered far field along the three previously defined directions.

where $\underline{\mathbf{F}}$ represents (5) with $R = 0$ term removed from the integration. Also, in the first inner product term of the right hand sided of (27), the positive sign is used when $\mathbf{r} \in S_d$ and $v = e$ and negative sign otherwise.

The next step in the MoM procedure is to substitute current expansion functions defined in (17) into (22)–(24), and this procedure yields the following set of equations given by

$$\sum_{n=1}^{N_c+N_d} A_{mn,e} I_n\left(t_j - \frac{R_{mn}^{\pm\pm}}{c_e}\right) + \sum_{n=1}^{N_c+N_d} B_{mn,e} \cdot \int_{\tau=0}^{t_j-(R_{mn}^{\pm\pm}/c_e)} I_n(\tau)\,d\tau + \sum_{n=1}^{N_d} C_{mn,e} M_n\left(t_j - \frac{R_{mn}^{\pm\pm}}{c_e}\right) = F_{m,j} + \sum_{n=1}^{N_c+N_d} A_{mn,e} I_n\left(t_{j-1} - \frac{R_{mn}^{\pm\pm}}{c_e}\right) \tag{28}$$

for $m = 1, 2, \ldots N_c + N_d$ and

$$\sum_{n=1}^{N_d} A_{mn,d} I_n\left(t_j - \frac{R_{mn}^{\pm\pm}}{c_d}\right) + \sum_{n=1}^{N_d} B_{mn,d} \int_{\tau=0}^{t_j-(R_{mn}^{\pm\pm}/c_d)} \cdot I_n(\tau)\,d\tau + \sum_{n=1}^{N_d} C_{mn,d} M_n\left(t_j - \frac{R_{mn}^{\pm\pm}}{c_d}\right) = \sum_{n=1}^{N_d} A_{mn,d} I_n\left(t_{j-1} - \frac{R_{mn}^{\pm\pm}}{c_d}\right) \tag{29}$$

for $m = 1, 2, \ldots, N_d$. In (28) and (29), we have

$$A_{mn,v} = \mu_v \int_S \int_S \frac{\mathbf{f_m} \cdot \mathbf{f_n}}{4\pi|\mathbf{r} - \mathbf{r}'|}\,dS'\,dS \tag{30}$$

$$B_{mn,v} = \frac{\Delta t}{\varepsilon_v} \int_S \int_S \frac{\nabla \cdot \mathbf{f_m}}{4\pi|\mathbf{r} - \mathbf{r}'|}\,dS'\,dS \tag{31}$$

$$C_{mn,v} = \pm \frac{\Delta t}{2} \langle \mathbf{f_m} \cdot \mathbf{f_n} \rangle + \Delta t \int_S \int_S \mathbf{f_m} \cdot \nabla \times \left[\frac{\mathbf{g_n}}{4\pi|\mathbf{r} - \mathbf{r}'|}\right] dS'\,dS \tag{30}$$

for $v = e$ or $v = d$ and

$$F_{m,j} = (\Delta t) \int_S \mathbf{f_m} \cdot \mathbf{E}^{\mathrm{inc}}(\mathbf{r}, t_j)\,dS. \tag{33}$$

Again note that, in (32) the first term on the right-hand side is positive if $\mathbf{r} \in S_d$ and $v = e$, and negative otherwise.

The integrals in (30)–(33) can now be evaluated by invoking the triangular basis functions. This results in

$$A_{mn,v} = \mu_v \frac{\ell_m}{2}\left[\boldsymbol{\rho}_m^{c+} \cdot \int_S \frac{\mathbf{f}_n}{4\pi\left|\mathbf{r}_m^{c+} - \mathbf{r}'\right|}\,dS' + \boldsymbol{\rho}_m^{c-} \cdot \int_S \frac{\mathbf{f}_n}{4\pi\left|\mathbf{r}_m^{c-} - \mathbf{r}'\right|}\,dS'\right] \tag{34}$$

$$B_{mn,v} = \frac{\Delta t}{\varepsilon_v}\,\frac{\ell_m}{2}\left[\int_S \frac{\nabla_s \cdot \mathbf{f}_n}{4\pi\left|\mathbf{r}_m^{c+} - \mathbf{r}'\right|}\,dS' + \int_S \frac{\nabla_s \cdot \mathbf{f}_n}{4\pi\left|\mathbf{r}_m^{c-} - \mathbf{r}'\right|}\,dS'\right] \tag{35}$$

$$F_{m,j} = \frac{(\Delta t)\ell_m}{2}\left[\boldsymbol{\rho}_m^{c+}\cdot\mathbf{E}^{\text{inc}}\left(\mathbf{r}_m^{c+}, t_j\right) + \boldsymbol{\rho}_m^{c-}\cdot\mathbf{E}^{\text{inc}}\left(\mathbf{r}_m^{c-}, t_j\right)\right] \tag{36}$$

by replacing the double integrals by single integrals on the primed variables and adopting a one point integration at the centroid of the respective triangles for the unprimed variables.

Last, we consider the inner product term in (32). We note that if edges m and n do not lie on a common triangle, then the result is zero. If they lie on a common triangle T, then let us assume for illustration the $m, n = 1, 2,$ or 3 as in Fig. 4. The contribution from T to the inner product is

$$\begin{aligned}\frac{\Delta t}{2}\left\langle\frac{\boldsymbol{\rho}_\mathbf{m}}{h_m}, \frac{\boldsymbol{\rho}_\mathbf{n}}{h_n}\right\rangle_T &= \frac{\Delta t}{2h_m h_n}\int_T \boldsymbol{\rho}_\mathbf{m}\cdot\boldsymbol{\rho}_\mathbf{n}\, dS \\ &= \frac{(\Delta t)\ell_m\ell_n}{8A}\left[\frac{|\mathbf{r_1}|^2+|\mathbf{r_2}|^2+|\mathbf{r_3}|^2}{12}\right. \\ &\left. \quad -(\mathbf{r_m}+\mathbf{r_n})\cdot\mathbf{r_c}+\mathbf{r_m}\cdot\mathbf{r_n}+\frac{3|\mathbf{r_c}|^2}{4}\right]\end{aligned} \tag{37}$$

where ℓ_m, r_c, and A represent the length of the mth edge, position vector to the centroid of the triangle, and area of the triangle T, respectively.

Next, we consider the left-hand sides of (28) and (29). Upon close examination, it is clear that depending on the choice of Δt, many terms under the summation signs are known and can be moved to the right-hand side. These are the terms for which $(R_{mn}^{\pm\pm}/c_v) \geq \Delta t$. Moving these terms to right-hand side, we can develop a single matrix equation given by

$$[\alpha]\left[\mathbf{X}(t_j)\right] = \left[\mathbf{Y}(t_j)\right] + [\beta]\left[\mathbf{X}\left(t_{j-1} - \frac{R_{mn}^{\pm\pm}}{c_v}\right)\right]. \tag{38}$$

Note that the elements of $[\alpha]$ matrix in (38) are formed by the potential terms when $(R_{mn}^{\pm\pm}/c_v) < \Delta t$. Furthermore, note that the $[\alpha]$ matrix is a sparse matrix and its sparsity depends upon the choice of Δt. Also, the elements of the matrix α_{mn} are not functions of time and, hence, need to be computed only once at the first time step. We also note that the computation of the elements of $X(t_{j-1} - (R_{mn}^{\pm\pm}/c_v))$ involves some type of interpolation in time. In this work, we simply chose linear interpolation although more complex interpolations are possible. Finally, the equivalent electric and magnetic currents induced on the scatterer may be obtained at each time step by solving (38).

V. Evaluation of the Far Scattered Fields

Once the transient currents on the scatterer have been determined, we can calculate the far scattered fields. These fields may be thought of as the superposition of the fields due to the electric currents only and with the fields due to the magnetic currents only.

The scattered magnetic field due to the electric currents alone at a point $\mathbf{r}$ is given by

$$\mathbf{H}_\mathbf{J}^\mathbf{s}(\mathbf{r}, t) = \frac{1}{\mu}\nabla\times\mathbf{A} = \frac{1}{\mu}\nabla\times\frac{\mu}{4\pi}\int_S \frac{\mathbf{J}\left(\mathbf{r}', t-\frac{R}{c_e}\right)}{R}\, dS' \tag{39}$$

where $R = |r - r'|$. Taking the curl operator inside the integral results in

$$\mathbf{H}_\mathbf{J}^\mathbf{s}(\mathbf{r}, t) = \frac{1}{4\pi}\int_S \cdot\left[\frac{\nabla\times\mathbf{J}\left(\mathbf{r}', t-\frac{R}{c_e}\right)}{R} - \frac{\hat{\mathbf{a}}_\mathbf{r}}{R^2}\times\mathbf{J}\left(\mathbf{r}', t-\frac{R}{c_e}\right)\right] dS'. \tag{40}$$

Since we are restricting ourselves to the far field, $R^2 \gg R$, so we can neglect the second term in (40). Further, we may write

$$\nabla\times\mathbf{J}\left(\mathbf{r}', t-\frac{R}{c_e}\right) = \frac{1}{c_e}\frac{\partial\mathbf{J}}{\partial t_r}\times\hat{\mathbf{R}} \tag{41}$$

where $t_r = t - (R/c_e)$, and $\hat{\mathbf{R}}$ is a unit vector in the direction $\mathbf{r}-\mathbf{r}'$. Therefore

$$\mathbf{H}_\mathbf{J}^\mathbf{s}(\mathbf{r}, t_n) \approx \sum_{k=1}^{N_e}\frac{1}{4\pi c_e}\frac{\partial I_k(t_r)}{\partial t_r}\int_{T_k^+ + T_k^-}\frac{\mathbf{f_k}\times\hat{\mathbf{R}}}{R}\, dS' \tag{42}$$

where N_e represents all the edges. For far-field calculations, we can make the following approximations: $R \approx r$, for magnitude terms where $r = |\mathbf{r}|$, $R \approx \mathbf{r} - \mathbf{r}'\cdot\hat{\mathbf{a}}_r$. The time derivative of the current is approximated with a finite difference as shown in (43) at the bottom of the page and the integral may be carried out analytically to give

$$\int_{T_k^+ + T_k^-}\frac{\mathbf{f_k}\times\hat{\mathbf{a}}_\mathbf{r}}{r}\, dS' = \frac{\ell_k}{2r}\left(\boldsymbol{\rho}_\mathbf{k}^{\mathbf{c}+} + \boldsymbol{\rho}_\mathbf{k}^{\mathbf{c}-}\right)\times\hat{\mathbf{a}}_\mathbf{r}. \tag{44}$$

Finally, combining (42)–(44), the normalized far magnetic field is given by (45) at the bottom of the next page and the electric field

$$\mathbf{E}_\mathbf{J}^\mathbf{s}(\mathbf{r}, t_n) = \eta_e\mathbf{H}_\mathbf{J}^\mathbf{s}(\mathbf{r}, t_n)\times\hat{\mathbf{a}}_\mathbf{r} \tag{46}$$

where η_e is the wave impedance in the medium surrounding the scatterer and the subscript J refers to the electric currents.

$$\frac{\partial I_k(t_r)}{\partial t_r} \approx \frac{I_k\left(t_{n+(1/2)} - \frac{r-\mathbf{r}'\cdot\hat{\mathbf{a}}_\mathbf{r}}{c_e}\right) - I_k\left(t_{n-(1/2)} - \frac{r-\mathbf{r}'\cdot\hat{\mathbf{a}}_\mathbf{r}}{c_e}\right)}{\Delta t} \tag{43}$$

We designate (45) and (46) as

$$\mathbf{H_J^s} = H^s_{J,\theta}\hat{\mathbf{a}}_\theta + H^s_{J,\phi}\hat{\mathbf{a}}_\phi \tag{47}$$

$$\mathbf{E_J^s} = \eta_e(H^s_{J,\phi}\hat{\mathbf{a}}_\theta - H^s_{J,\theta}\hat{\mathbf{a}}_\phi). \tag{48}$$

The scattered fields from the magnetic current is given by

$$\mathbf{E_M^s}(\mathbf{r}, t) = \frac{-1}{\varepsilon_e}\nabla\times\mathbf{F_e} = \frac{-1}{\varepsilon_e}\nabla\times\frac{\varepsilon_e}{4\pi}\int_S \frac{\mathbf{M}\left(\mathbf{r}', t - \dfrac{R}{c_e}\right)}{R}\,dS' \tag{49}$$

where the M subscript refers to the magnetic currents. By following a similar analysis as that for the electric currents, we can show (50) at the bottom of the page and

$$\mathbf{H_M^s}(\mathbf{r}, t_n) = \frac{1}{\eta_e}\hat{\mathbf{a}}_\mathbf{r}\times\mathbf{E_M^s}(\mathbf{r}, t_n) \tag{51}$$

$$\mathbf{E_M^s} = E^s_{M,\theta}\hat{\mathbf{a}}_\theta + E^s_{M,\phi}\hat{\mathbf{a}}_\phi \tag{52}$$

$$\mathbf{H_M^s} = \frac{1}{\eta_e}(-E^s_{M,\phi}\hat{\mathbf{a}}_\theta + E^s_{M,\theta}\hat{\mathbf{a}}_\phi). \tag{53}$$

Finally, the total fields scattered from the dielectric body may be obtained by adding (48) and (52), and (47) and (53) to obtain

$$\mathbf{E_{tot}^s} = (\eta_e H^s_{J,\phi} + E^s_{M,\theta})\hat{\mathbf{a}}_\theta + (-\eta_e H^s_{J,\theta} + E^s_{M,\phi})\hat{\mathbf{a}}_\phi \tag{54}$$

$$\mathbf{H_{tot}^s} = (H^s_{J,\theta} - \frac{1}{\eta_e}E^s_{M,\phi})\hat{\mathbf{a}}_\theta + (H^s_{J,\phi} + \frac{1}{\eta_e}E^s_{M,\theta})\hat{\mathbf{a}}_\phi. \tag{55}$$

VI. Numerical Results

Typical numerical results are presented for EM scattering from complex composite structures. The first structure considered in this section is an aircraft. The nose part of the aircraft is made of dielectric shown in Fig. 1 and the remainder of the structure is conducting. The dielectric constant of the nose has $\varepsilon_r = 10.0$, $\sigma = 0$ and $\mu_r = 1$. It is illuminated by a Gaussian plane wave which is given by

$$\mathbf{E}^{\text{inc}}(\mathbf{r}, t) = \mathbf{E_0}\frac{4}{T\sqrt{\pi}}e^{-\gamma^2} \tag{56}$$

where

$$\gamma = \frac{4}{T}(ct - ct_0 - \mathbf{r}\cdot\hat{\mathbf{k}}) \tag{57}$$

with $E_o = \pm\hat{\mathbf{a}}_\mathbf{x}$, $\mathbf{k} = -\hat{\mathbf{a}}_\mathbf{z}$, $T = 30.0$ ℓm and $\mathrm{ct}_o = 45.0$ ℓm. (The unit ℓm denotes a light meter. A light meter is the length of time taken by the EM wave to travel 1 m. Assuming the medium to be free space this amounts to 1 $\ell\mathrm{m} = 3.335\,64$ ns.) The field is incident nose on and is arriving from $\phi = 0°$ and $\theta = 0°$. The incident electric field is x-polarized. The time step ($c\Delta t = 3.0$ ℓm) is chosen larger than the time step given by the Courant condition in order to generate the implicit solution.

We first consider the transient currents at several points (on the dielectric nose, conduction bodies, tails, and wings). The transient electric currents on the conducting structures are given in Fig. 8(a). The magnetic and electric currents on the dielectric structures are shown in Fig. 8(b) and (c) along with the incident electric field, respectively.

Finally, the far-radiated electric field from the structure is plotted in Fig. 9 for different angles of scattering. Fig. 9(a) plots the x component of the scattered electric far fields along $\phi = 0;\ \theta = 0$ (back side), $\phi = 0;\ \theta = 180°$ (forward) and $\phi = 90°;\ \theta = 90°$ (side). Fig. 9(b) depicts the y component of the electric far-fields along the three previously mentioned directions. Observe that the y component of the field along the side is approximately zero. Finally, Fig. 9(c) provides the z component of the far scattered fields along the three previously defined directions. Please note that only in the side direction is the z component significant.

Second structure that is presented is a helicopter shown in Fig. 10 and its whole body is conductor. A Gaussian plane wave is given with $\mathbf{E}_o = \pm\hat{\mathbf{a}}_\mathbf{x}$, $\mathbf{k} = -\hat{\mathbf{a}}_\mathbf{z}$, $T = 72.0$ ℓm, and $ct_o = 108.0$ ℓm. The field is incident on the top and is arriving from $\phi = 0°$ and $\theta = 0°$, x polarized, and with the time step $c\Delta t = 5.4$ ℓm. We also consider the transient currents at four points (on the head, body, wing, and tail), and the transient electric currents on the structure are given in Fig. 11. Observe that all the currents on both structures are stable in the late time.

VII. Conclusion

Analysis of transient scattering from composite complex structures is carried out by solving a set of coupled TDIEs. The TDIEs are derived using the equivalence principle and utilizing the continuity conditions on the electric field. For a numerical solution, we employ the MoM in conjunction with

$$r\mathbf{H_J^s}(\mathbf{r}, t_n) = \frac{1}{4\pi}\sum_{k=1}^{N_e}\left[\frac{I_k\left(t_{n+(1/2)} - \dfrac{r - \mathbf{r}'\cdot\hat{\mathbf{a}}_\mathbf{r}}{c_e}\right) - I_k\left(t_{n-(1/2)} - \dfrac{r - \mathbf{r}'\cdot\hat{\mathbf{a}}_\mathbf{r}}{c_e}\right)}{c\Delta t}\right]\cdot\frac{\ell_k}{2r}\left(\boldsymbol{\rho}_\mathbf{k}^{\mathbf{c}+} + \boldsymbol{\rho}_\mathbf{k}^{\mathbf{c}-}\right)\times\hat{\mathbf{a}}_\mathbf{r} \tag{45}$$

$$r\mathbf{E_M^s}(\mathbf{r}, t_n) = \frac{-1}{4\pi}\sum_{k=1}^{N_e}\left[\frac{M_k\left(t_{n+(1/2)} - \dfrac{r - \mathbf{r}'\cdot\hat{\mathbf{a}}_\mathbf{r}}{c_e}\right) - M_k\left(t_{n-(1/2)} - \dfrac{r - \mathbf{r}'\cdot\hat{\mathbf{a}}_\mathbf{r}}{c_e}\right)}{c\Delta t}\right]\cdot\frac{\ell_k}{2r}(\rho_\mathbf{k}^{\mathbf{c}+} + \rho_\mathbf{k}^{\mathbf{c}-})\times\hat{\mathbf{a}}_\mathbf{r} \tag{50}$$

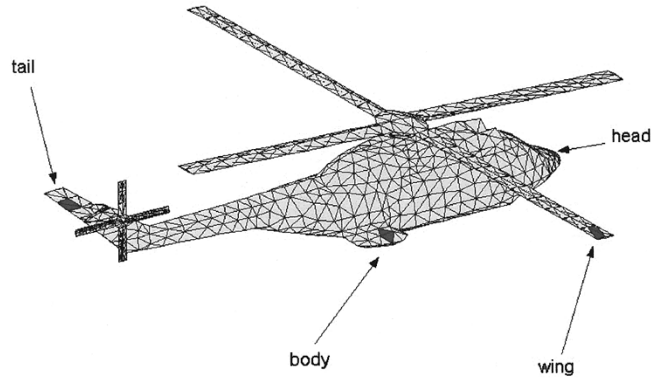

Fig. 10. A helicopter and the locations where the transient currents are computed.

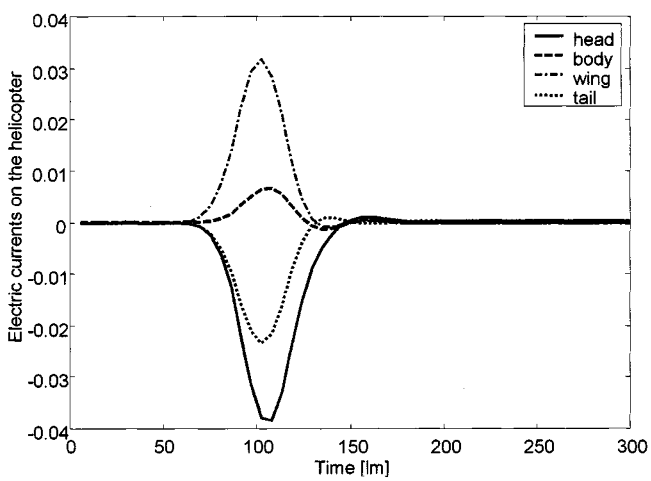

Fig. 11. Electric currents on the helicopter.

planar triangular patch modeling. The method presented can either be explicit or implicit depending upon the duration of the time step. Please note that, in order for the solution to be explicit the time step must be less than $R_{\min}/c_e$ where $R_{\min}$ and c_e represent the minimum distance between any two patches and the velocity of the EM wave in the external medium, respectively. However, explicit solutions are known to develop instabilities for late time and, for this reason we choose an implicit scheme which provides a stable solution.

REFERENCES

[1] E. M. Kennaugh and R. L. Cosgriff, "The use of impulse response in electromagnetic scattering problems,", IRE Nat. Convention Record, 1958.

[2] V. H. Weston, "Pulse return from a sphere," *IRE Trans. Antennas Propagat.*, vol. AP-7, pp. S43–S51, Dec. 1959.

[3] T. T. Wu, "Transient response of a dipole antenna," *J. Math. Phys.*, vol. 2, no. 6, pp. 892–894, 1961.

[4] L. B. Felsen, "Diffraction of the pulsed field from an arbitrarily oriented electric or magnetic dipole by a perfectly conducting wedge," *SIAM J. Appl. Math.*, vol. 26, no. 2, pp. 306–312, 1974.

[5] R. H. Schafer and R. G. Kouyoumjian, "Transient currents on a cylinder illuminated by an impulsive plane wave," *IEEE Trans. Antennas Propagat.*, vol. AP-23, pp. 627–638, Sept. 1975.

[6] K. K. Chan and L. B. Felsen, "Transient and time-harmonic diffraction by a semi-infinite cone," *IEEE Trans. Antennas Propagat.*, vol. AP-25, pp. 802–806, Nov. 1977.

[7] A. K. Dominek, "Transient scattering analysis for a circular disk," *IEEE Trans. Antennas Propagat.*, vol. 39, pp. 815–819, June 1991.

[8] C. L. Bennett, "A technique for computing approximate electromagnetic impulse response of conducting bodies," Ph.D. dissertation, Purdue Univ., West Lafayette, IN, Aug. 1968.

[9] S. M. Rao, T. K. Sarkar, and S. A. Dianat, "A novel technique to the solution of transient scattering from thin wires," *IEEE Trans. Antennas Propagat.*, vol. 36, pp. 1188–1192, Aug. 1988.

[10] N. J. Damaskos, R. T. Brown, J. R. Jameson, and P. L. E. Uslenghi, "Transient scattering by resistive cylinders," *IEEE Trans. Antennas Propagat.*, vol. 33, pp. 21–25, Jan. 1985.

[11] D. A. Vechinski and S. M. Rao, "Transient scattering by conducting cylinders—The case," *IEEE Trans. Antennas Propagat.*, vol. 40, pp. 1103–1106, Sept. 1992.

[12] C. L. Bennett and H. Mieras, "Transient scattering from open thin conducting surfaces," *Radio Sci.*, pp. 1231–1239, 1981.

[13] E. K. Miller and J. A. Landt, "Direct time domain techniques for transient radiation and scattering from wires," *Proc. IEEE*, vol. 68, pp. 1396–1427, Nov. 1980.

[14] C. L. Bennett and G. F. Ross, "Time domain electromagnetics and its applications," *Proc. IEEE*, vol. 66, pp. 299–318, Mar. 1978.

[15] S. M. Rao and D. R. Wilton, "Transient scattering by conducting surfaces of arbitrary shape," *IEEE Trans. Antennas Propagat.*, vol. 39, pp. 56–61, Jan. 1991.

[16] A. G. Tijhuis, *Electromagnetic Inverse Profiling: Theory and Numerical Implementation*: VNU, 1987.

[17] D. A. Vechinski and S. M. Rao, "Transient scattering from two-dimensional dielectric cylinders of arbitrary shape," *IEEE Trans. Antennas Propagat.*, vol. 40, pp. 1054–1060, Sept. 1992.

[18] ——, "Transient scattering from two-dimensional dielectric cylinders: E-field, H-field and combined field solutions," *Radio Sci.*, pp. 611–622, 1992.

[19] H. Mieras and C. L. Bennett, "Space-time integral equation approach to dielectric targets," *IEEE Trans. Antennas Propagat.*, vol. 30, pp. 2–9, Jan. 1982.

[20] S. M. Rao, D. R. Wilton, and A. W. Glisson, "Electromagnetic scattering by surfaces of arbitrary shape," *IEEE Trans. Antennas Propagat.*, vol. AP-30, pp. 409–418, May 1982.

[21] B. P. Rynne, "Time domain scattering from arbitrary surfaces using the electric field integral equation," *J. Electromagn. Waves Applicat.*, vol. 5, pp. 93–112, Jan. 1991.

[22] D. A. Vechinski and S. M. Rao, "Transient scattering from dielectric cylinders—E-field, H-field, and combined field solutions," *Radio Sci.*, vol. 27, pp. 611–622, Sept./Oct. 1992.

[23] B. P. Rynne and P. D. Smith, "Stability of time marching algorithms for the electric field integral equation," *J. Electromagn. Waves Applicat.*, vol. 4, pp. 1181–1205, Dec. 1990.

[24] B. P. Rynne, "Instabilities in time marching methods for scattering problems," *Electromagn.*, vol. 4, pp. 129–144, 1986.

[25] A. G. Tijhuis, "Toward a stable marching-on-in-time method for two-dimensional transient electromagnetic scattering problems," *Radio Sci.*, vol. 19, pp. 1311–1317, Sept./Oct. 1984.

[26] E. Arvas, A. Rahhal-Arabi, A. Sadigh, and S. M. Rao, "Scattering from multiple conducting and dielectric bodies of arbitrary shape," *IEEE Trans. Antennas Propagat. Mag.*, vol. 33, pp. 29–36, Apr. 1991.

[27] P. D. Smith, "Instabilities in time marching methods for scattering: Cause and rectification," *Electromagn.*, vol. 10, pp. 439–451, 1990.

[28] G. Manara, A. Momorchio, and R. Reggiannini, "A space-time discretization criterion for a stable time-marching solution of the electric field integral equation," *IEEE Trans. Antennas Propagat.*, vol. 45, pp. 527–532, Mar. 1997.

[29] S. M. Rao, D. A. Vechinski, and T. K. Sarkar, "Transient scattering by conducting cylinders—Implicit solution for transverse electric case," *Microwave Opt. Technol. Lett.*, vol. 21, pp. 129–134, Apr. 1999.

[30] R. F. Harrington, *Field Computation by Moment Methods*. Malabar, FL: Krieger, 1982.

[31] K. M. Mitzner, "Numerical solution from a hard surface of arbitrary shape—Retarded potential technique," *J. Acoust. Soc. Amer.*, vol. 42, pp. 391–397, 1967.

[32] R. P. Shaw, "Diffraction of acoustic pulses by obstacles of arbitrary shape with a robin boundary condition," *J. Acoust. Soc. Amer.*, vol. 41, pp. 855–859, 1967.

[33] M. D. Pocock and S. P. Walker, "Radar cross section prediction using boundary integral equation methods with isoparametic quadratic surface modeling and iterative solvers," *Electromagn.*, vol. 16, pp. 651–669, 1996.

[34] M. D. Pocock, M. J. Bluck, and S. P. Walker, "Electromagnetic scattering from 3-D curved dielectric bodies using time-domain integral equations," *IEEE Trans. Antennas Propagat.*, vol. 46, pp. 1212–1219, Aug. 1998.

Tapan Kumar Sarkar (S'69–M'76–SM'81–F'92) received the B.Tech. degree from the Indian Institute of Technology, Kharagpur, India, in 1969, the M.Sc.E. degree from the University of New Brunswick, Fredericton, NB, Canada, in 1971, and the M.S. and Ph.D. degrees from Syracuse University, Syracuse, NY, in 1975.

From 1975 to 1976, he was with the TACO Division of the General Instruments Corporation. He was with the Rochester Institute of Technology, Rochester, NY, from 1976 to 1985. He was a Research Fellow at the Gordon McKay Laboratory, Harvard University, Cambridge, MA, from 1977 to 1978. He is now a Professor in the Department of Electrical and Computer Engineering, Syracuse University; Syracuse, NY. He has authored or coauthored more than 210 journal articles and numerous conference papers and has written 28 chapters and ten books including the latest one *Iterative and Self Adaptive Finite-Elements in Electromagnetic Modeling* (Norwood, MA: Artech House, 1998). He is on the editorial board of *Journal of Electromagnetic Waves and Applications* and *Microwave and Optical Technology Letters*. His current research interests deal with numerical solutions of operator equations arising in electromagnetics and signal processing with application to system design.

Dr. Sarkar is a Registered Professional Engineer in the State of New York. He received the Best Paper Award of the IEEE TRANSACTIONS ON ELECTROMAGNETIC COMPATIBILITY in 1979 and at the 1997 National Radar Conference. He obtained one of the "Best Solution" Awards in May 1977 at the Rome Air Development Center (RADC) Spectral Estimation Workshop. He received the College of Engineering Research Award in 1996 and the chancellor's citation for excellence in research in 1998 at Syracuse University. He was an Associate Editor for feature articles of the IEEE Antennas and Propagation Society Newsletter and he was the Technical Program Chairman for the 1988 IEEE Antennas and Propagation Society International Symposium and URSI Radio Science Meeting. He has been appointed U.S. Research Council Representative to many URSI General Assemblies. He was the Chairman of the Intercommission Working Group of International URSI on Time-Domain Metrology (1990–1996). He is a member of Sigma Xi and International Union of Radio Science Commissions A and B. He received the title *Docteur Honoris Causa* from Universite Blaise Pascal, Clermont Ferrand, France, in 1998 and the Medal of the City Clermont Ferrand, France, in 2000.

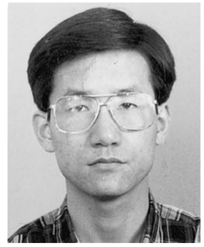

Wonwoo Lee was born in Pusan, Korea. He received the B.S. degree in electrical engineering from Korea Military Academy, Korea, in 1989 and the M.S. degree in electrical engineering from Sogang University, Seoul, Korea, in 1993. He is currently working toward the Ph.D. degree in electrical engineering from Syracuse University, Syracuse, NY.

From 1993 to 1997, he was a Lecturer and Assistant Professor in the Department of Electrical Engineering of Korea Military Academy, Korea. He is currently a Research Assistant in the Computational Electromagnetics Laboratory, Syracuse University. His current interests include numerical analysis of scattering and radiation problems from complex structure.

Sadasiva M. Rao (M'83–SM'90–F'00), photograph and biography not available at time of publication.